Proximity effect and electron transport in oxide hybrid heterostructures with superconducting/magnetic interfaces

G A Ovsyannikov[1,2], K Y Constantinian[1], Yu V Kislinski[1], A V Shadrin[1], A V Zaitsev[1], A M Petrzhik[1], V V Demidov[1], I V Borisenko[1], A V Kalabukhov[2] and D Winkler[2]

[1] Kotel'nikov Institute of Radio Engineering and Electronics, Russian Academy of Sciences, 125009 Moscow, Russia
[2] Department of Microtechnology and Nanoscience, Chalmers University of Technology, SE-412 96 Gothenburg, Sweden

E-mail: gena@hitech.cplire.ru

Abstract
We report on electron transport in oxide heterostructures with superconducting/magnetic (S/M) thin film interfaces. The investigated hybrid mesa-heterostructures consist of a cuprate superconductor, a nonsuperconducting cuprate (antiferromagnetic) or manganite (ferromagnetic) interlayer with thickness $d_M = 5$–50 nm and a conventional superconductor (Nb). The superconducting critical current (I_C) with a critical current density $j_c = 10^3$ A cm^{-2} (for $d_M = 10$ nm) and a characteristic voltage $I_C R_N = 100$–200 μV (R_N is normal resistance) are observed at liquid helium temperature for a $Ca_X Sr_{1-X} CuO_2$ antiferromagnetic cuprate interlayer with a thickness of $d_M = 10$–50 nm. The superconducting current-phase relation of heterostructures deviates from the regular sine type, demonstrating a second harmonic component. These hybrid heterostructures with S/M interfaces show unusually high sensitivity to external magnetic fields. When substituting the cuprate interlayer by a manganite film, no critical current was observed although the manganite interlayer was made several times thinner (down to $d_M \leqslant 5$ nm).

1. Introduction

Coexistence of superconducting and magnetic ordering in solids is of great interest for fundamental physics and electronic applications. The exchange mechanism of ferromagnetic ordering tends to align spins of superconducting pairs in the same direction, preventing singlet pairing [1, 2]. At the interfaces between superconducting (S) and magnetic matter (M), however, the superconducting and magnetic correlations may interact due to the proximity effect (penetration of superconducting correlations into magnetic matter) resulting in interplay between superconducting and magnetic ordering, and novel physical phenomena may appear. However, up to now most of the activity was devoted to investigations of structures where the M interlayer is a ferromagnetic (F) one. One of the important properties of the proximity effect at the S/F interface is a damped oscillatory

behaviour of the superconducting wavefunction induced in the F interlayer. This may lead, in particular, to a π-phase shift [3] in the superconducting current-phase relation (CPR) of S/F/S Josephson junctions, experimentally demonstrated in [4]. In some structures, for instance, in F/S/F spin-valve junctions one can use the F interlayer to control the superconductivity by a magnetic field or the electric current affecting the exchange interactions in F electrodes [5]. Much less attention was paid to superconducting structures with an M interlayer having antiferromagnetic (AF) ordering. Recently Gor'kov and Kresin [6] assumed a model (GK model) of the S/AF/S structure where an AF interlayer consists of F layers with magnetizations aligned perpendicular to the surface of the S electrodes and the biasing current directed along the layers. The GK model predicts the existence of critical current like in a structure with spacing between S electrodes larger than the coherence length ξ_N in normal metal. The GK model

also predicts that even a minor change in canting of magnetic moments in the F layers caused by an external magnetic field will reduce the critical current. The authors of the work [7] considered an M interlayer as a series of F layers with in-plane parallel magnetization, and showed that the Josephson critical current significantly depends on whether the number of F layers is odd or even.

Theoretical investigation of an S/M/S structure with an M interlayer composed of N F layers, each one with a thickness significantly exceeding the atomic scale (magnetic multilayer structure, MMS), was carried out in the work [8]. The orientation of the F layer magnetizations in the MMS model was parallel to the S/M interface. It was shown that for AF ordering of the F layers in MMS the long-range proximity effect will take place at the S/M interface and the amplitude of the Josephson current in S/M/S depends on the number of F layers.

Recently experimental observation of the Josephson effect in Nb/Cu/FeMn/Nb polycrystalline thin film multilayer structures has been demonstrated in [9], where γ-Fe$_{50}$Mn$_{50}$ alloy (FeMn) is used as a metallic AF interlayer. Significant suppression of superconductivity has been observed in the S/AF bilayer with an FeMn layer and the critical current modulation with magnetic field $I_C(H)$ of the S/AF/S structure shows a rather conventional Fraunhofer pattern [9]. If instead of using a polycrystalline metallic AF material one would substitute it by an array of F layers with alternating directions of magnetization, according to the GK model the dependence $I_C(H)$ should then exhibit rapid oscillations. Recently experimental observations of such oscillations and the critical current dependence on M-interlayer thickness have been shown [10–12].

In order to observe the proximity effect in a superconducting structure with an M interlayer, a transparent S/M interface is needed. This is also why in-depth investigations of such interfaces composed of cuprate superconductor and antiferromagnetic cuprate are highly relevant [13, 14]. However, in spite of promising progress in the fabrication of heterostructures with M interlayer [10–16], there is still a lack of experimental results on Josephson junctions with an AF interlayer, in particular with cuprate material. At the same time the mutual influence of antiferromagnetism and d-wave superconductivity at S/M interfaces in Josephson junctions is necessary to unveil.

In this paper we report on the experimental studies of the dc and rf current transport through superconducting/magnetic interfaces realized in hybrid Nb/Au/M/YBa$_2$Cu$_3$O$_{7-\delta}$ mesa-heterostructures (MHS) with the in-plane size L varied from 10 to 50 μm. Here bilayer Nb/Au is a conventional s-wave superconductor (S$'$) and YBa$_2$Cu$_3$O$_{7-\delta}$ (YBCO) is a cuprate superconductor with dominating d-wave order parameter (S$_d$). The M interlayer is either Ca$_{1-x}$Sr$_x$CuO$_2$ (CSCO) ($x = 0.15$ or 0.5), which is a quasi-two-dimensional Heisenberg antiferromagnetic cuprate [17, 18], or a mixed-valence manganite La$_{1-y}$Ca$_y$MnO$_3$ (LCMO) exhibiting both antiferromagnetism if $y = 0$, and ferromagnetism if $y = 0.3$ [19]. We also summarize recently obtained results on the proximity effect and electron transport in hybrid

heterostructures with an M/S$_d$ interface taking into account the experimental data published elsewhere [10–12, 20].

The structure of experimental samples, the fabrication details and measurement techniques are presented in section 2. X-ray diffraction data of the reference (deposited directly on substrate) M films and heterostructures, their electrical and magnetic properties are discussed in section 3. The superconducting transport properties in MHS are discussed in section 4, where the dynamic behaviour at microwave frequencies and the measurements of the superconducting current-phase relation are presented. Section 5 contains the comparison of the calculations using the MMS model with experiment. The long-range proximity effect is discussed. Experimental magnetic field dependences of the superconducting current are compared with the GK model. In the conclusions we summarize the obtained results.

2. Experimental technique

The double-layer epitaxial thin film structures M/YBCO were grown *in situ* by pulsed-laser ablation on (110) NdGaO$_3$ (NGO) substrates. The c axis of the M/YBCO heterostructures is perpendicular to the substrate surface. Typically, the $d_M = 5$–100 nm thick M films were deposited on top of 150 nm thick YBCO films. M interlayers were either Ca$_{1-x}$Sr$_x$CuO films ($x = 0.15$ and 0.5) or La$_{1-y}$Ca$_y$MnO$_3$ ($y = 0$ and 0.3) as possible candidates for the magnetic interlayer, as recommended in [6][3]. The M/YBCO heterostructures were covered *in situ* by a 10–20 nm thick Au film and afterwards a 200 nm thick Nb film was deposited *ex situ* by dc-magnetron sputtering in an Ar atmosphere. In order to fabricate the Nb/Au/M/YBCO mesa structure we utilized photolithography, reactive plasma etching and Ar ion-milling techniques. An SiO$_2$ protective layer was deposited by rf-magnetron sputtering and patterned afterwards in order to define the mesa area. An additional 200 nm thick Nb/Au bilayer film was deposited on top of the MHS and patterned in order to form the superconducting wiring. The square S$'$/N/M/S$_d$ MHS having areas $A = L^2$ from 10×10 μm^2 and up to 50×50 μm^2 were fabricated (see figure 1).

For comparison, a similar fabrication procedure was used for structuring of the MHS without an M interlayer [21]. In order to avoid pinholes the deposited M films were usually thicker than the surface roughness of the YBCO layer. For an M interlayer with thickness 2–5 nm the NbBa$_2$Cu$_3$O$_{7-\delta}$ (NBCO) films were used instead of YBCO since it has a smoother surface. Peak-to-valley surface roughness of (001) YBCO films measured by atomic force microscopy were 2–5 nm, and 1–2 nm for the heterostructures based on NBCO. Direct Nb deposition on top of the YBCO film results in formation of an Nb/YBCO interface with very high resistance ($\sim$1 Ω cm^2) due to the Nb film oxidation. Thus, if the Au layer is locally damaged because of the finite surface roughness of the M/S$_d$ interface then niobium oxide is directly formed there, also preventing pinhole formation in MHS.

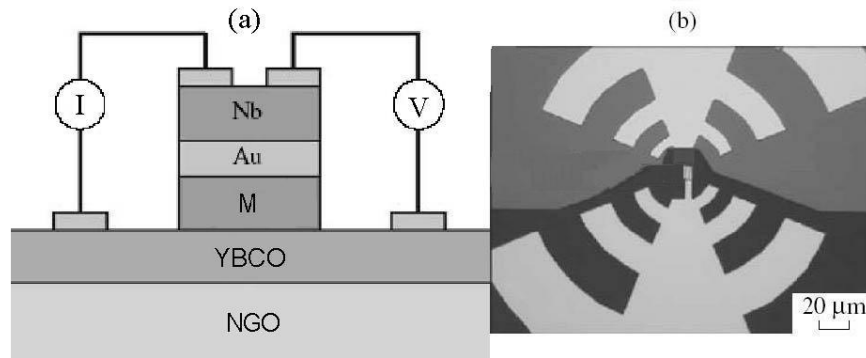[3] La$_{0.7}$Sr$_{0.3}$MnO$_3$ (LSMO) interlayer is used for comparison.

Figure 1. The cross section of the MHS and the current biasing circuit (a). The layer thicknesses are as follows: YBCO—150 nm, M interlayer—5–100 nm, Au—10–20 nm, Nb—200 nm. The contacts to the YBCO and Nb films are made by additional Au layer with thickness 100 nm. Top view of MHS incorporated in log periodic antenna (b). A space bar of 20 μm is shown for scale.

Table 1. The crystal parameters for heterostructures and reference M films.

Structure	CSCO $x = 0.15$	CSCO/YBCO $x = 0.15$		CSCO $x = 0.5$	CSCO/YBCO $x = 0.5$		LMO	LMO/YBCO	
Reflection	(002)	(002)	(007)	(002)	(002)	(007)	(002)	(002)	(007)
peak	CSCO	CSCO	YBCO	CSCO	CSCO	YBCO	LMO	LMO	YBCO
$a_\perp$ [a] (nm)	0.321	0.322	1.169	0.333	0.336	1.177	0.398	0.397	1.171
$\Delta\omega$ [b] (deg)	0.07	0.2 [c]	0.2 [c]	0.4	0.5 [c]	0.5 [c]	0.06	0.4	0.4

[a] $a_\perp$ is the lattice *c*-axis crystal parameter. [b] $\Delta\omega$ is full width at half-maximum of the rocking curve. [c] The estimation of $\Delta\omega$ was made from 2θ–ω scan.

3. Crystal structure and resistance of the interlayer

3.1. X-ray diffraction analysis

The XRD 2θ–ω scans for the CSCO (and manganite LMO) epitaxial films deposited both on the (110) NGO substrate (reference film) and on the YBCO/NGO heterostructure show the presence of (001) CSCO (LMO) film without extra phases [12]. The rocking curve measurements of the full width at half-maximum ($\Delta\omega$) of the (002) peak for the reference CSCO film ($x = 0.15$) deposited directly on the NGO substrate revealed a narrow peak with $\Delta\omega = 0.07°$. That value is smaller than $\Delta\omega = 0.2°$ of the (007) peak measured for the best YBCO film. The rocking curve measurement of the single-crystal substrate (110) NGO showed $\Delta\omega = 0.006°$ determined by the resolution of the x-ray diffractometer [12, 22]. FWHM $\Delta\omega$ values of the rocking curve of the CSCO film deposited on YBCO films are increased by several times.

Similar behaviour is observed for CSCO ($x = 0.5$) and for LMO films deposited on the YBCO/NGO heterostructure (see table 1). All M films deposited on the YBCO/NGO heterostructures demonstrate a broadening of the rocking curve, manifested in a reduction of crystallographic quality and in a minor change of the lattice constants. Experiment [13] showed that in the La-based cuprate interface the upper limit on possible cation intermixing is less than 1 nm. According to [23, 24] the interfaces in cuprate/manganite might be coherent, free of defects, exhibiting roughness less than 1 nm and there is no major chemical ion intermixing. However, x-ray absorption spectroscopy analysis of the interface shows some cation displacement [25].
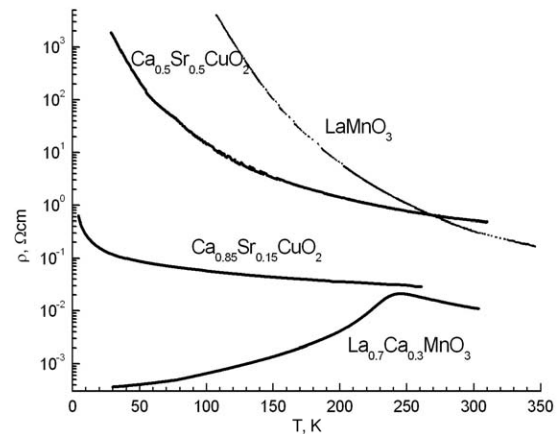

Figure 2. Temperature dependences of the specific resistance of reference M films with the thickness 80 nm.

3.2. M-film resistance

Temperature dependences of the specific resistance (ρ) of the reference M films are presented in figure 2. Increasing ρ is observed with lowering the temperature (T) for all M films, with the exception of La$_{1-y}$Ca$_y$MnO$_3$ ($y = 0.3$), which shows a metal–insulator transition at $T_{MI} \approx 250$ K. Note that the LCMO films have lower resistance than other M films at room temperature. The temperature dependences of the resistance of CSCO, LMO and LCMO films (for $T > T_{MI}$) correspond well to the variable-range hopping model (see [22] and references in it):

$$\rho(T) = \rho_0 \exp(T_0/T)^{1/4}, \qquad (1)$$

where ρ_0 and T_0 are experimental parameters. According to the 3D hopping model $T_0 = (ce/k_B)/N(E_f)\lambda^3$, where c is constant, k_B is the Boltzmann constant, $N(E_f)$ is the density of states at the Fermi level and λ is the localization distance. The localization distance $\lambda \approx 1$ nm was estimated for CSCO (with $x = 0.5$) taking the constant $c \approx 20$ from percolation theory and $[N(E_f)\lambda^3]^{-1} \approx 10$ eV for $T_0 = 3 \times 10^6$ K at $T = 300$ K. Note that the activation energy $E_{hop} = k_B T (T_0/T)^{1/4}$ in our case is somewhat smaller than the gap, defined from optical measurements [26]. No activation-type dependence was observed for M-film resistance even at $\rho > 10^3$ Ω cm.

3.3. Magnetic properties of M films

The magnetic sublattice of M films is defined by their crystal structure. It is known that the magnetic sublattices of CSCO and LMO correspond to the G- and A-type AF ordering where ferromagnetic layers are parallel to the crystallographic planes (111) CSCO and (001) LMO, respectively [17–19]. We used the electron paramagnetic resonance (EPR) spectrometer to obtain the temperature dependence of electromagnetic spectra of the films under study. The temperature dependences of both resonance fields and areas of absorption lines at 3 cm microwaves were investigated. The paramagnetic spectrum from Mn^{2+} of a reference sample Mn: MgO placed into the same microwave cavity was measured simultaneously to exclude any changes of the recording system. However, we were not able to resolve the paramagnetic resonance line of CSCO films with the EPR technique approach. Moreover, much more sensitive measurements using a SQUID magnetometer also did not help in determining the Néel temperature (T_N) because of too high magnetic moments of the Nd ions in the NGO substrate used for fabrication of the CSCO thin films. The results of neutron studies [17, 18] obtained on polycrystalline samples gave $T_N = 540$ K. Using data for manganite films (see, for example, [23–25]) we expect that T_N doesn't change significantly for our epitaxial CSCO films with $d_M > 10$ nm. Therefore, we assumed that the CSCO films are in a G-type antiferromagnetic state at experimental temperatures $T = 4.2$–40 K. This could be considered as the magnetic multilayer structure.

A ferromagnetic resonance (FMR) for reference LCMO films (with a thickness down to 10 nm) was observed. Curie temperature $T_{CU} \approx 200$ K of the LCMO film is not far from the temperature of the metal–insulator transition T_{MI} that is typical for manganites.

Although the temperature dependences of the resistance of LMO films do not demonstrate a resistive metal–insulator transition (see figure 2), the FMR spectrum shows ferromagnetic resonance with $T_{CU} \approx 140$ K both for the LMO films deposited directly on NGO substrates and on YBCO/NGO heterostructures. It is commonly accepted that the double-exchange interaction between Mn^{3+} and Mn^{4+} ions are responsible for ferromagnetism in doped manganites like LCMO [19]. For low doped compositions the super-exchange interaction between Mn^{3+} ions is responsible for the appearance of FM and AFM phases. Jahn–Teller distortion plays an important role in the ordering of Mn^{3+} ions [27, 28],
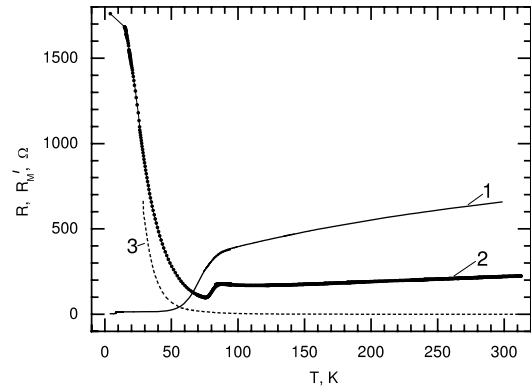

Figure 3. Temperature dependence of resistance $R(T)$ for MHSs with CSCO interlayer ($x = 0.5$): (curve 1)—$d_M = 12$ nm, $L = 10$ μm, and (curve 2)—$d_M = 80$ nm, $L = 50$ μm. Curve 3 shows the expected contribution of interlayer resistance $R'_M = \rho_M d_M/L^2$ for $d_M = 80$ nm, $L = 50$ μm when ρ_M has been calculated from the resistance of the reference film (figure 2).

and ferromagnetism is observed both in the low doped $La_{1-x}Mn_{1-x}O_3$ compounds and in the $LaMnO_{3+\delta}$ with an oxygen nonstoichiometry. The strain of the manganite films due to the influence of the substrate [29] can enhance the ferromagnetism in LMO similar to ferromagnetism induced by external pressure [27].

4. Electron transport in heterostructures with M/S interfaces

4.1. Temperature dependence of hybrid heterostructure resistance

The resistance of MHS measured at low bias voltages is the sum of the resistances:

$$R = R_{YBCO} + R_{M/Y} + R'_M + R_b + R_{Nb/Au} + R_{Nb} + R_{Au}, \quad (2)$$

where R_{YBCO} comes from the YBCO electrode, $R_{M/Y}$ is the M/YBCO interface resistance, R'_M is the resistance of the M interlayer, R_b is the Au/M interface barrier resistance, and the resistances R_{Nb} and R_{Au} come from the Nb electrode and Au film, respectively. The contribution of the thin Au film can be neglected [21]. At temperatures higher than the superconducting critical temperature ($T_c = 70$–80 K) of the YBCO film ($T > T_c$) the temperature dependence of the MHS resistance $R(T)$ is similar to the reference YBCO film (decreases with T) as seen in figure 3. For samples with a thick CSCO interlayer ($d_M > 100$ nm) a large deviation from the linear decrease in $R(T)$ was observed. At $T'_c < T < T_c$ (where $T'_c = 8$–9 K is the critical temperature of the Nb/Au bilayer) the MHS resistance is determined by the resistance of the interfaces M/YBCO, Au/M, Nb/Au and Nb wiring, and the resistance of the M interlayer R'_M. Independently measured specific resistance of the Nb/Au interface ($\sim 10^{-11}$ Ω cm^2) [21] results in ~ 1 $\mu\Omega$—a negligibly small contribution to the total resistance of MHS. Taking into account the epitaxial growth of the CSCO/YBCO structure, and similar parameters of the crystal structure of contacting materials, one can assume that
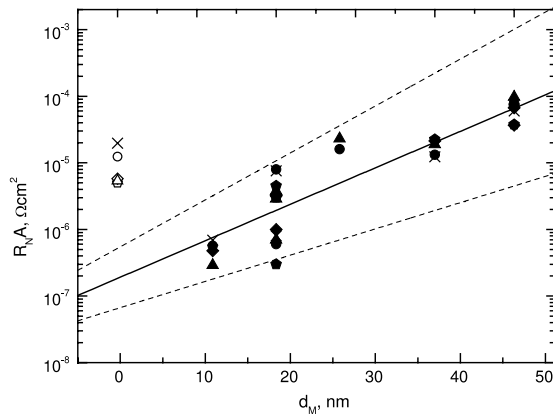
Figure 4. M-interlayer thickness (d_M) dependence of specific resistance ($R_N A$) for MHS with CSCO, $x = 0.5$ at $T = 4.2$ K. The data for MHS with the size L and $d_M \geqslant 10$ nm are indicated by filled symbols: crosses—$L = 10\ \mu$m, circles—$20\ \mu$m, triangles—$30\ \mu$m, rhombuses—$40\ \mu$m, pentagons—$50\ \mu$m. Open symbols correspond to the case $d_M = 0$. The exponential increase of the $R_N A$ resistance with decay length $\sim$8 nm is shown by the solid line, while thin dashed lines indicate the confidence interval.

Figure 5. Temperature dependence of resistance $R(T)$ for MHS with three types of M interlayer: LMO (1)—point-dashed line, LCMO (2)—dashed line and LSMO (3)—solid line. The resistance is normalized to the resistance at $T = 278$ K.

interface resistance $R_{M/Y}$ is small compared to the resistance R_b of the Au/CSCO interface as a metal/oxide interface [21]. From the data shown in figure 2 we see that the reference CSCO film ($x = 0.5$) deposited on the NGO substrate shows $\rho = 10^3$–$10^4\ \Omega$ cm at low temperatures ($T < 50$ K) resulting in an expected contribution of the M film to the resistance R of the MHS of more than 1 kΩ. However, for MHS with a thin CSCO interlayer $d_M < 50$ nm no increase of resistance R was observed. Compared to the reference CSCO films (figure 2) the resistance of the MHS at $T'_c < T < T_c$ (curve 1 in figure 3) is weakly dependent on temperature and is significantly smaller than the resistance of the CSCO interlayer $R'_M = \rho_M d_M / A$ ($A = L^2$ is the MHS area) obtained from measurements of specific resistance of the reference CSCO film. The contribution of R'_M appears at $d_M > 100$ nm.

The specific resistance $R_N A$ of the MHS measured at bias voltage $V \geqslant 2$ mV and $T = 4.2$ K exponentially increases with d_M (see also [12]). Figure 4 presents the dependence of specific resistance $R_N A$ for MHS with CSCO, $x = 0.5$. All data are given for samples which demonstrate the Josephson effect and nonzero critical current. Variation in planar size L of MHS does not influence the exponential dependence of $R_N A(d_M)$. Again, if the main contribution to $R_N A$ comes from M-interlayer resistance, then a linear increase of $R_N A$ with d_M should be observed. In thin films ($d_M < 80$ nm) oxygen nonstoichiometry may give a rearrangement of the electronic subsystem [30–32], changing the CSCO interlayer conductivity and resulting in the exponential dependence of $R_N A(d_M)$. Similarly, as was shown in [13], despite weak cation diffusion (about 1–2 unit cells) at the interfaces of two cuprates, the changing of conductivity in cuprates could be caused by electronic rearrangement or oxygen nonstoichiometry as it happens at the interface of a strongly correlated Mott and a band insulator [32]. Charge rearrangement may lead to a significant alteration of the electronic subsystem, and may cause the transition of
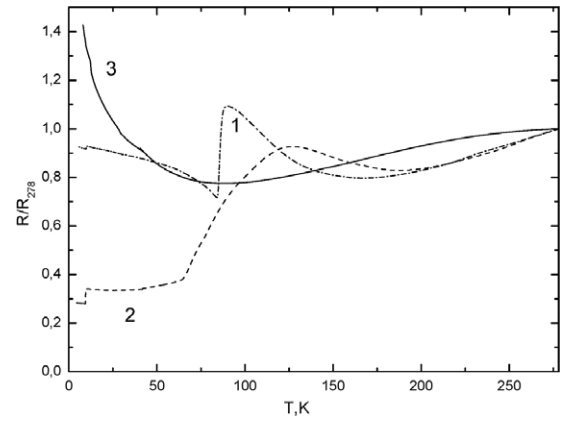
a thin ($d_M < 50$ nm) CSCO layer into the metallic state, as was observed in [33] with decreasing the oxygen content in the CSCO film during its growth. A significant change in the electronic conductivity can occur due to the interaction between the oxygen atoms in the CSCO/YBCO interface, leading to the observed dependence of $R(T)$ in the temperature range $T < T_c$. That is to say, the non-uniform electron doping across the interlayer thickness can explain the exponential dependence of $R_N A(d_M)$ (figure 4). The main contribution to the MHS resistance comes from the Au/CSCO interface. Data in figure 4 show that MHS with $d_M < 40$ nm have smaller $R_N A$ than $R_N A$ of samples without an M interlayer ($d_M = 0$). The possible reason could be the sensitivity of the YBCO surface to the oxygen content that we also observed in the case of the Nb/YBCO interface [21]. Note, our estimations for current influenced by the tunnelling in the M interlayer is exponentially small due to large thickness, $d_M > 10$ nm. The electrical conductivity of MHS at high voltages (up to 100 mV) resembles tunnelling-type transport, and thus differs from the conductivity known for ballistic superconducting contacts or superconducting junctions with a normal metal interlayer. This feature is presumably due to the presence of an Au/CSCO interface with low transparency.

The temperature dependences of the resistance for three MHSs with a manganite interlayer with $d_M > 10$ nm are presented in figure 5. At high temperatures $T > 200$ K the $R(T)$ dependences (for LMO and LCMO interlayers) are determined mainly by the YBCO electrode as for MHS with a CSCO interlayer (see figure 3). Small distortion from linear dependence of $R(T)$ for MHS with an LSMO interlayer is caused by high Curie temperature $T_{CU} \geqslant 300$ K. Resistance drops at T around 100 K are aroused either by superconductivity of YBCO or a metal–insulator transition for MHS with a manganite interlayer. Small variation of $R(T)$ at $T < T'_c$ is induced by superconductivity of the Nb/Au bilayer. Contribution of the manganite layer and the S/M interfaces to the resistance of the MHS dominates at $T \leqslant T_c$. In the case of LMO, the interlayer resistance increases monotonically with

Table 2. DC parameters of MHS with $Ca_{X-1}Sr_XCuO_{7-\delta}$ M interlayer measured at $T = 4.2$ K.

Sample no.	x^a	d_M^b (nm)	L^c (μm)	I_C^d (μA)	R_N^e (Ω)	V_c^f (μV)	q^g
1	0.15	50	10	44	3.0	132	0.2
2	0.15	20	10	49	1.9	93	0.08
3	0.5	20	10	334	0.71	237	0.4
4	0.5	50	10	2.5	60	150	0.13
5	—	0	40	160	0.36	58	0.5
6	—	0	20	18	3.6	65	0.4

[a] x is the Sr doping level of CSCO. [b] d_M is the thickness of the M interlayer ($d_M = 0$ corresponds to the absence of an interlayer). [c] L is linear size of MHS. [d] I_C is the critical current. [e] R_N is the normal resistance. [f] $V_c = I_C R_N$. [g] $q = I_{c2}/I_C$ is the ratio of the amplitude of the second harmonic in the CPR to critical current.

lowering the temperature, although the increase is slower than in the case of the reference LMO film (see figure 2).

The resistance of the LMO interlayer, calculated from ρ of the reference film (figure 2), is higher than the MHS resistance with the same interlayer. So, we observed a significant reduction of resistance of the LMO film in the MHS configuration. The similar reduction of resistance of MHS with a CSCO M interlayer was discussed earlier. At $T < T_{MI}$ the contribution of the LCMO interlayer to the resistance of MHS is small due to a metal–insulator transition of the LCMO film. Specific resistance for the reference LCMO film at $T = 4.2$ K is $\rho_M = 10^{-3}$ Ω cm. The contribution of these films to MHS specific resistance is small: $\rho_M d_M = 10^{-9}$ Ω cm^2, while $R_N A \approx 2 \times 10^{-4}$ Ω cm^2 for $d_M = 10$ nm.

Thickness dependences of $R_N A$ (averaged values over five junctions with the planar sizes from $L = 10$–50 μm on a chip) for MHS with LMO and LCMO interlayers are shown in figure 6. The R_N resistances were taken from I–V curves at $V \geqslant 2$ mV where the influence of the Nb energy gap is minimized. In spite of the large spread of parameters the specific resistance $R_N A$ of MHS with manganite shows a polynomial increase with d_M, shown by a solid line in figure 6. The expected contribution from M-interlayer resistance $\rho_M d_M$ calculated from ρ_M at $T = 4.2$ K for reference manganite films (see figure 2) is shown by dashed lines. Thus, at low temperatures $T < T_c'$ the resistance of MHS with an LMO interlayer is determined by the interfaces between superconductor and M interlayer. The investigated MHS could be considered as an $S'/I_1/M/I_2/S_d$ structure, where the I_1 and I_2 are the barriers at the Au/M and M/YBCO interfaces, correspondingly. Taking the estimated maximal resistance of the Au/manganite interface [34] and assuming that the contribution of M-layer resistance is small, we find that the determining factor in MHS resistance comes from the manganite/YBCO interface (transparency of barrier I_1, is much higher than for I_2).

4.2. Superconducting current

The superconducting current (I_C) is clearly observed at $T = 4.2$ K for MHS with a CSCO interlayer with thickness $d_M = 10$–50 nm both for $x = 0.5$ and 0.15 (see table 2). Data in table 2 show that the $I_C R_N$ products are higher than the $I_C R_N$ of MHS without an M interlayer ($d_M = 0$), where the reason for the superconducting current is a non-vanishing
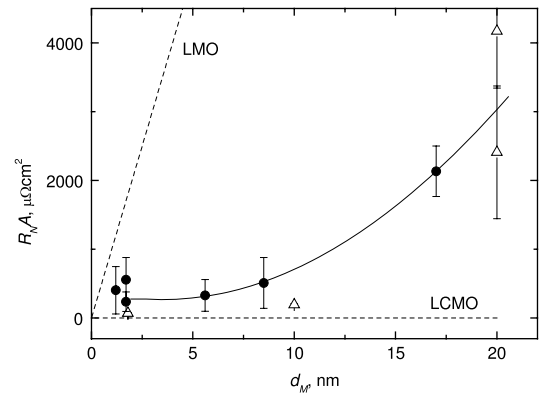

Figure 6. Thickness dependence of MHS specific resistance ($R_N A$): with LMO (filled circles) and LCMO (triangles) interlayers. The spread bars indicate $R_N A$ variation for 5 MHS on each chip. A polynomial approximation of $R_N A(d_M)$ is shown by a solid line. Possible contributions of M-interlayer resistance $\rho_M d_M$ are shown by dashed lines calculated using data for reference LCMO and LMO films at $T = 4.2$ K (see figure 2).

admixture of s-wave pairing in YBCO (see [21] and references there). Assuming high transparency D_1 for the barrier of the CSCO/YBCO interface the MHS can be considered as $S'/I_B/M/S_d$ structures, where the barrier I_B is formed due to structural defects, nonstoichiometry at the Au/CSCO interface and the difference of Fermi velocities for the contacting materials [21]. Impact of the M/S_d interface on Δ_d and Δ_S pair potentials could be essential. As follows from [35] Δ_d could rapidly decrease while Δ_S may increase at the M/S_d interface. Since I_C is proportional to Δ_S [21] its increasing leads to I_C increasing.

The $I_C(T)$ curves follow the temperature dependence of the Nb superconducting gap similar to the case of MHS without an M interlayer [10, 21]. Such behaviour also follows from calculations [8] of the long-range proximity effect in the M interlayer. However, we did not observe either any noticeable change of the $I_C R_N$ product from the thickness of the CSCO layer, or a square-law increase of critical current with decreasing temperature T near T_c' [10].

The MHS with the M interlayer made of manganite film had no critical current although the thickness of d_M was reduced down to 5 nm. For LCMO as well as LMO interlayers at $d_M < 3$ nm critical current appears in MHS just due to pinholes in the M interlayer. Magnetic and microwave

characteristics of MHS with pinholes differ significantly from the behaviour for a lumped Josephson junction described, in particular, by the resistive shunted junction (RSJ) model [36]. Note, pinholes were observed for some MHS with a thin CSCO interlayer (d_M < 5 nm). These measurements show that LCMO/YBCO and LMO/YBCO interface transparencies (D_2) are significantly smaller than for CSCO/YBCO ($D_1 \ll 1$). So, in the case of a manganite M interlayer we deal with the MHS with two low-transparent barriers that strongly suppress the critical current I_C being proportional to the product $D_1 D_2$ [37].

Thus, the absence of critical current for the MHS with a manganite M interlayer with thicknesses as small as d_M < 5 nm even at $T = 0.3$ K is, probably, caused by a combination of the ferromagnetism of M layers and the presence of a barrier with low transparency at the M/S_d interface. However, we observed some peculiarities in conductivity σ (V) at low voltage V < 1 mV like those published in [38, 39] but they cannot be clearly identified by Andreev bound states or a resonant proximity effect [40].

4.3. Current-phase relation of the superconducting current in MHS with CSCO/YBCO interface

The dominant d-wave along with s-wave symmetries of the superconducting order parameter in the S_d electrode may result in a non-sinusoidal CPR for MHS with c-axis-oriented YBCO, which contains first (I_{c1}), second (I_{c2}), etc harmonics, i.e. $I_S(\varphi) = I_{c1} \sin\varphi + I_{c2} \sin 2\varphi + \cdots$. Note, the d-wave component may give a second harmonic in CPR which is proportional to the second order of transparency D of the barrier in the c-oriented S/S_d contact ($I_{c2} \propto D^2$) [41–45]. The values of the second harmonics were defined from measurements of Shapiro steps, which arise on the I–V curves under electromagnetic irradiation at any experimental frequency in the range 36–120 GHz. All MHS demonstrated Shapiro steps with strong modulation as a function of the microwave power (inset to figure 7). The modulation of the amplitudes of the Shapiro steps versus applied microwave power confirms the Josephson origin of the superconducting current. Less than 20% difference has been observed between the critical frequency $f_c = 2eV_c/h = 71$ GHz calculated from $V_c = I_C R_N = 147$ μV (static estimation of f_c) and the $f_c = 56$ GHz determined from the maximum value of the first Shapiro step using the RSJ model approach (dynamic f_c) [36]. The correspondence between these two (dynamic and static) values of f_c clearly indicates the absence of pinholes [16]. The deviation of the experiment from model calculations becomes smaller if we take into account the presence of the second harmonic component in the CPR, which is manifested by fractional Shapiro steps (inset to figure 7) observed at all experimental frequencies up to 120 GHz.

It is known that the fractional Shapiro steps may also originate from some additional reasons like nonhomogeneous superconducting current distribution, resonant interaction of the Josephson oscillation with nonlinearity of the quasiparticle current or finite capacitance C of the Josephson junction [21, 36]. The homogeneous superconducting current distribution was checked by magnetic field dependences of the
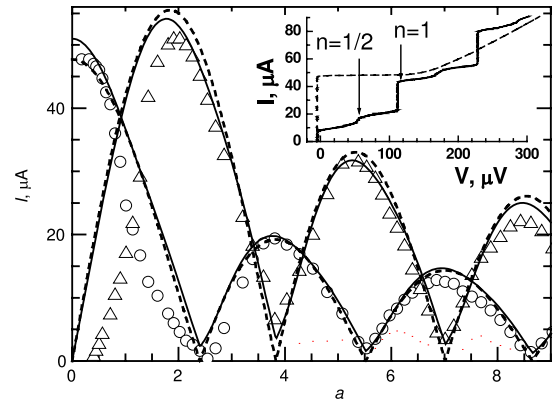

Figure 7. The critical current I_C (circles) and first Shapiro step I_1 (triangles) versus normalized $a = I_e/I_C$ microwave current I_e for MHS #1. $T = 4.2$ K, microwave frequency $f_e = 56$ GHz. The solid lines correspond to the $I_C(a)$ and $I_1(a)$ curves numerically calculated from the modified RSJ model taking into account the second harmonic in CPR for $q = 0.2$, dashes—for $q = 0$ [21]. I–V curves with (solid line) and without (dashes) external microwaves are shown in the inset. Positions of integer $V_1 = nhf_e/2e$ ($n = 1$) and half-integer $n = 1/2$ Shapiro steps are indicated by arrows.

critical current (see section 5.2). The strong nonlinearity of the quasiparticle current at voltage range $V \geqslant hf_e/2e$ was not observed for MHS. Capacitance C (McCumber parameter $\beta_c = 2e/hI_C R_N^2 C = 2$–6) was estimated from the hysteretic I–V curves. In order to investigate the influence of the second harmonic in the CPR and the capacitance C on dynamic properties of MHS we have studied dependences of the critical current $I_C(a)$ and the first Shapiro step $I_1(a)$ versus normalized amplitude $a = I_e/I_C$ of the external electromagnetic radiation (figure 7). The microwave current amplitudes (a) were determined in the RSJ model approach from the attenuation levels of applied microwave power [21, 36]. The performed calculations of the Shapiro step amplitudes based on the modified RSJ model taking into account the β_c parameter in the high-frequency limit $f_e/f_c \gg 1$ or $a \gg 1$ show that at frequencies $f_e > f_c$ the impact of capacitance C on the Shapiro step amplitudes is small, and the $I_C(a)$ and $I_1(a)$ dependences are determined mainly by the first and second harmonics of the CPR. The experimental data presented in figure 7 are fitted well to the theoretical dependences calculated taking into account the amplitude I_{c2} of the second harmonic in the CPR $q = I_{c2}/I_C = 0.2$. A deviation of $I_C(a)$ and $I_1(a)$ dependences from the theoretical curves at small amplitudes of the microwave power $a \leqslant 2$ could be attributed to a weak fulfilment of the high-frequency limit for the case $f_e/f_c = 0.88$. Note, the sign of q can be determined by analysing the experimental dependence of half-integer Shapiro step $I_{1/2}(a)$ in comparison with the theoretical calculated one [21]. This procedure gives us negative $q < 0$. The negative sign of the second harmonic in the CPR is native for superconducting junctions with a d-wave order parameter [35, 43–45]. Assuming $I_{c2} \propto D^2$, and low transparency coefficients $D \ll 1$ estimated from $R_N A$ products, one may expect vanishing I_{c2} amplitudes. At the same time in accordance with [46] an admixture of d-wave and s-wave components results in the appearance of the

second harmonic in CPR in S/S_d contacts. Thus, in our MHS the d-wave component of the pair potential also exists at the Au/CSCO interface due to the proximity effect.

5. Proximity effect at AF/S interface

5.1. Thickness dependence

Figure 8 shows the experimental and the calculated critical current density (j_c) dependence on the thickness (d_M) of the M interlayer for different levels of exchange field ($J_{ex}/\pi k_B T$). Presented in the figure, data show no impact of planar size L on the overall exponential decrease of j_c with d_M, similar to the exponential increase of $R_N A$ as shown in figure 4. The calculations of $j_c(d_M)$ were done within the MMS model [12] of the S'/I$_B$/M/S structure, where I$_B$ is a barrier with low transparency and both S' and S are s-wave superconductors (inset to figure 8). It is assumed that the M interlayer consists of N ferromagnetic F layers each one with a thickness $d = d_M/N$ much larger than the interatomic distance. The value of the layer exchange energy J_{ex} is assumed to be small compared with the Fermi energy. Magnetizations of layers are assumed to be collinear and have orientation in the plane of the M/S interface. The considered model enables us to use the approach based on quasiclassical Green's function equations (see, e.g., [1, 2]). For the chosen fitting parameters, $N = 20$ and $J_{ex}/\pi k_B T = 2$, the decay depth corresponds to $\xi_{AF} = 7 \pm 1$ nm. Thus, in the CSCO interlayer the decay depth ξ_{AF} significantly exceeds the coherence length of the polycrystalline metallic AF interlayer FeMn [9]. Statistical analysis of experimental data obtained from the $j_c(d_M)$ dependences also gives values of ξ_{AF} close to 7–9 nm. Note, theoretical dependences have been calculated for identical singlet s-wave superconductors, but the results remain qualitatively unchanged for different superconductors S and S'. In the experiment the superconductors were not identical; moreover, in the YBCO electrode the s-wave symmetry is not dominant. The theoretical curves demonstrate decreasing j_c with increasing exchange energy J_{ex}. A different behaviour for j_c is seen for structures with even and odd N.

Following the analysis of the S$_d$/M interfaces in [21, 35, 41, 43], the amplitude of the superconducting current in the structures between the s-wave superconductor and a mixed (s + d)-wave superconductor is determined mostly by the contribution of the s-wave component. Presence of an s-wave component in the S$_d$ electrode (Δ_S) determines the critical current of MHS which is proportional to the product $\Delta_S \Delta_{Nb}$. However, the theoretical model does not describe resistive features of the MHS with a CSCO interlayer, namely the exponential increase of the specific resistance $R_N A$ with d_M (see section 4.1) and the deviation of the CPR from the sine type (see section 4.3).

5.2. Magnetic sensitivity

According to the GK model [6] for an S/AF/S structure (a sketch for the model is given in the inset to figure 9), the critical current I_C depends on the canting of magnetization M_S in the
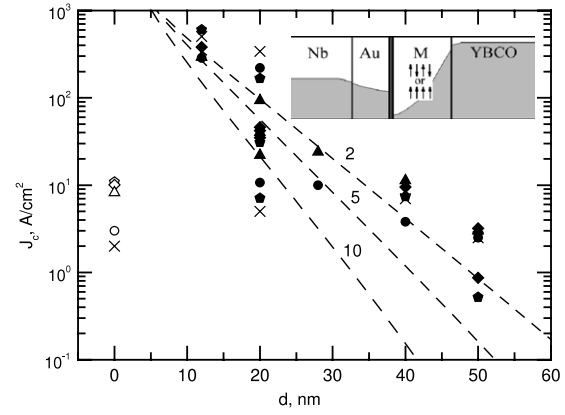

Figure 8. Thickness dependence of experimental superconducting current density for MHS with the size L indicated by filled symbols: crosses—$L = 10$ μm, circles—20 μm, triangles—30 μm, rhombuses—40 μm, pentagons—50 μm, data for $d_M = 0$ are shown by open symbols of the same type. Dashed lines show calculations using the MMS model for AF ordering in the interlayer for different levels of exchange field $J_{ex}/\pi k_B T = 2$, 5 and 10. The coherence length of the CSCO ($x = 0.5$) interlayer estimated from fitting experimental data with theoretical $j_c(d_M)$ dependence for $J_{ex}/\pi k_B T = 2$ is $\xi_{AF} = 7 \pm 1$ nm. The MHS structure with MMS interlayer is shown in the inset. Variation of the superconducting pair potential is shown schematically.

layers induced, for example, by an external magnetic field H as follows:

$$I_c \approx I_c^0 \left(\frac{2}{\pi \beta M_S} \right)^{1/2} \left| \cos \left(\beta M_S - \frac{\pi}{4} \right) \right|. \quad (3)$$

The zeros of I_C correspond to the relation $\beta M_S = \pi/4 + \pi n$ ($n = 1, 2, \ldots$), where $\beta \gg 1$ depends on the electron hopping parameter. It is seen that the oscillations of I_C could be observed at small canting (determined by M_S in (3)) [6].

Figure 9 shows experimental $I_C(H)$ for the MHS with the CSCO interlayer. Supposing a linear dependence of M_S from an external magnetic field H the expected (3) dependence $I_C(H)$ is shown in figure 9. $I_C^0 = I_C(H = 0)$ and the magnetic field H_1 at the first zero of experimental $I_C(H)$ are fitting parameters. Experimental $I_C(H)$ differs significantly from the Fraunhofer pattern which is typical for the usual Josephson junctions (see [36]):

$$I_c(H) = I_c^0 \left| \frac{\sin(\pi \Phi/\Phi_0)}{\pi \Phi/\Phi_0} \right|, \quad (4)$$

where $\Phi = \mu_0 H A_{ef}$ is the magnetic flux through the MHS, μ_0 is a magnetic constant, $\Phi_0 = h/2e$ is the magnetic flux quantum, $A_{ef} = L d_e$, $d_e = \lambda_{L1} + \lambda_{L2} + d_M$ is effective penetration depth of the magnetic field, $\lambda_{L1} = 150$ nm and $\lambda_{L2} = 90$ nm are London penetration depths for the electrodes of the MHS and $d_M = 50$ nm is the interlayer thickness.

The applicability of equation (3) for a magnetic field close to $H = 0$ is limited [6], which results in the observed deviation of the experimental points from the solid line in figure 9. The absolute value of H_1 for the MHS with an M interlayer is significantly smaller than H_1 of the MHS
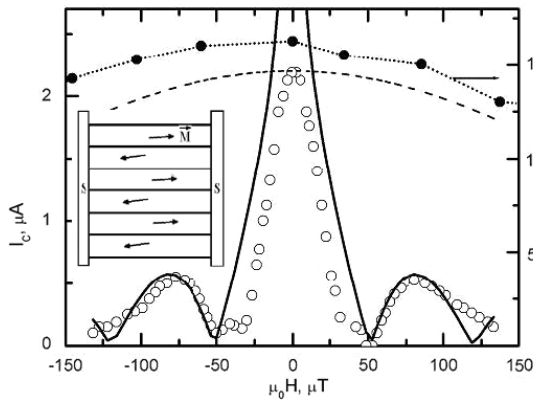
Figure 9. Magnetic field dependence of the critical current $I_C(H)$ (open circles) for an MHS with CSCO ($x = 0.5$), $d_M = 50$ nm, $L = 10$ μm at $T = 4.2$ K. The solid line shows the dependence (3) taking $I_C(0) = I_C^0$, and magnetic field H at the first minimum as a fitting parameter. The dashed line is the Fraunhofer dependence (4) calculated for $L = 10$ μm and the London penetration depths $\lambda_{L1} = 150$ nm and $\lambda_{L2} = 90$ nm for YBCO and Nb, correspondingly. Filled circles show experimental $I_C(H)$ dependence for the MHS without M interlayer with $L = 50$ μm. The inset shows a sketch of the GK model.

without an M interlayer (see filled circles in figure 9). The significant decrease in H_1 cannot be simply explained by a possible increase of the London penetration depth λ_{L1} in the YBCO due to a lower level of oxygen doping of the YBCO film near to the CSCO/YBCO interface seen from a decreased critical temperature of the YBCO film in MHS down to $T_c \approx 80$ K. Note, in accordance with the review [47] a minor increase (less than 30%) of λ_L may happen if the critical temperature of YBCO decreases to $T_c = 40$ K due to oxygen nonstoichiometry.

6. Summary

Our experimental studies of hybrid heterostructures with interfaces of cuprate superconductor/cuprate antiferromagnetic $Ca_X Sr_{1-X} CuO_2$ show the presence of long-range proximity effects and clear Josephson effects. The heterostructures had critical current densities up to 10^3 A cm^{-2} at $T = 4.2$ K and a characteristic voltage $V_c = 100$–200 μV independent of the thickness of the antiferromagnetic interlayer. The estimated experimental and theoretical penetration depths of superconducting correlations agreed well within experimental error, and significantly exceeded the values published for a polycrystalline antiferromagnetic interlayer. The second harmonic of the current phase relation of 10–40% of the critical current was evaluated via measurements of integer and half-integer Shapiro steps, and indicated the presence of d-wave superconductivity in the interlayer. Compared to ordinary Josephson junctions, these heterostructures show unusually high sensitivity to external magnetic fields, presumably caused by the influence of the external magnetic field on AF ordering of the magnetization in the M interlayer. The critical current was absent for the structures with a 5 nm thick manganite interlayer even at low temperatures, $T = 0.3$ K, due

to ferromagnetism in the interlayer. However, we do not exclude an influence of a sufficiently high barrier in the manganite/cuprate interface which limits the proximity effect in the heterostructure.

References

[1] Buzdin A I 2005 *Rev. Mod. Phys.* **77** 935
[2] Bergeret F S, Volkov A F and Efetov K B 2005 *Rev. Mod. Phys.* **77** 1321
[3] Bulaevskiǐ L N, Kuziǐ V V and Sobyanin A A 1977 *JETP Lett.* **25** 290
[4] Ryazanov V V, Oboznov V A, Rusanov A Yu, Veretennikov A V, Golubov A A and Aarts J 2001 *Phys. Rev. Lett.* **86** 2427
[5] Gu J Y, You C-Y, Jiang J S, Pearson J, Bazaliy Ya B and Bader S D 2002 *Phys. Rev. Lett.* **89** 267001
[6] Gor'kov L and Kresin V 2001 *Appl. Phys. Lett.* **78** 3657
    Gor'kov L and Kresin V 2004 *Phys. Rep.* **400** 149
[7] Andersen B M, Barash Yu S, Graser S and Hirschfeld P J 2008 *Phys. Rev.* B **77** 054501
    Andersen B M, Barash Yu S, Graser S and Hirschfeld P J 2006 *Phys. Rev. Lett.* **96** 117005
[8] Zaitsev A V 2009 *JETP Lett.* **90** 521
[9] Bell C, Tarte E J, Burnell G, Leung C W, Kang D-J and Blamire M G 2003 *Phys. Rev.* B **68** 144517
[10] Komissinskiy P V, Ovsyannikov G A, Borisenko I V, Kislinskii Yu V, Constantinian K Y, Zaitsev A V and Winkler D 2007 *Phys. Rev. Lett.* **99** 017004
[11] Kislinskii Y V, Constantinian K Y, Ovsyannikov G A, Komissinskiy P V, Borisenko I V and Shadrin A V 2008 *JETP* **106** 800
[12] Zaitsev A V, Ovsyannikov G A, Constantinian K Y, Kislinskii Y V, Shadrin A V, Borisenko I V and Komissinskiy P V 2010 *JETP* **110** 336
[13] Gozar A, Logvenov G, Kourkoutis L F, Bollinger A T, Giannuzzi L A, Muller D A and Bozovic I 2008 *Nature* **455** 782
[14] Bozovic I, Logvenov G, Verhoeven M A J, Caputo P, Goldobin E and Beasley M R 2004 *Phys. Rev. Lett.* **93** 157002
[15] Tarutani Y, Fukazawa T, Kabasawa U, Tsukamoto A, Hiratani M and Takagi K 1991 *Appl. Phys. Lett.* **58** 2707
[16] Barholtz K-U, Kupriyanov M Yu, Hubner U, Schmidl F and Seidel P 2000 *Physica* C **334** 175
[17] Vaknin D, Caignol E, Davisl P K, Fischer J E, Johnston D C and Goshorn D P 1989 *Phys. Rev.* B **39** 9122
[18] Matsumura M, Raffa F and Brinkmann D 1999 *Phys. Rev.* B **60** 6285
[19] Izyumov Yu A and Scryabin Yu N 2001 *Phys.—Usp.* **44** 109
[20] Ovsyannikov G A, Borisenko I V, Komissinski P V, Kislinski Yu V and Zaitsev A V 2006 *JETP Lett.* **84** 262

[21] Komissinskiy P V, Ovsyannikov G A, Constantinian K Y, Kislinski Y V, Borisenko I V, Soloviev I I, Kornev V K, Goldobin E and Winkler D 2008 *Phys. Rev.* B **78** 024501
[22] Ovsyannikov G A, Denisuk S A, Bdikin I K, Ivanov Z and Claeson T 2004 *Physica* C **408–410** 616
[23] Varela M, Lupini A R, Pennycook S J, Sefrioui Z and Santamaria J 2003 *Solid-State Electron.* **47** 2245
[24] Peña V, Sefrioui Z, Arias D, Leon C, Santamaria J, Varela M, Pennycook S J and Martinez J L 2004 *Phys. Rev.* B **69** 224502
[25] Stadler S, Idzerda Y U, Chen Z, Ogale S B and Venkatesan T 1999 *Appl. Phys. Lett.* **75** 3384
[26] Tokura Y, Koshihara S, Arima T, Takagi H, Ishibashi S, Ido T and Uchida S 1990 *Phys. Rev.* B **41** 11657
[27] Huang Q, Santoro A, Lynn J W, Erwin R W, Borchers J A, Peng J L and Greene R L 1997 *Phys. Rev.* B **55** 14987
[28] Fite I M, Szymczak R, Baran M B, Markovich V, Puzniak R, Wisniewski A, Shiryaev S V, Varyukhin V N and Szymczak H 2003 *Phys. Rev.* B **68** 014436
[29] Ovsyannikov G A *et al* 2009 *JETP* **108** 48
[30] Okamoto S and Millis A J 2004 *Nature* **428** 630
[31] Nie J C, Badica P, Hirai M, Kodama J Y, Crisan A, Sundaresan A, Tanaka Y and Ihara H 2003 *Physica* C **388/389** 441
[32] Billinge S J L, Davies P K, Egami T and Catlow C R A 1991 *Phys. Rev.* B **43** 10340
[33] Dorr K 2006 *J. Phys. D: Appl. Phys.* **39** R125
[34] Mieville L, Worledge D, Geballe T H, Contreras R and Char K 1998 *Appl. Phys. Lett.* **73** 1736
[35] Kuboki K 2000 *Physica* B **284–288** 505
[36] Barone A and Paterno G 1982 *Physics and Applications of the Josephson Effect* (New York: Wiley and Sons)
[37] Ovsyannikov G A and Babayan G E 1991 *Physica* B **168** 239
[38] Kraus P A, Bhattacharya A and Goldman A M 2001 *Phys. Rev.* B **64** 220505
[39] Chen Z Y, Biswas A, Zutic Ì, Wu T, Ogale S B, Greene R L and Venkatesan T 2001 *Phys. Rev.* B **64** 220505
[40] Yokoyama T, Tanaka Y and Golubov A A 2006 *Phys. Rev.* B **73** 094501
[41] Komissinski P V, Il'ichev E, Ovsyannikov G A, Kovtonyuk S A, Grajcar M, Hlubina R, Ivanov Z, Tanaka Y, Yoshida N and Kashiwaya S 2002 *Europhys. Lett.* **57** 585
[42] Golubov A, Kupriyanov M Yu and Il'ichev E 2004 *Rev. Mod. Phys.* **76** 411
[43] Lofwander T, Shumeiko V S and Wendin G 2001 *Supercond. Sci. Technol.* **14** R5
[44] Il'ichev E *et al* 2001 *Phys. Rev. Lett.* **86** 5369
[45] Amin M H S *et al* 2002 *Physica* B **318** 162
[46] Zhang W and Wang Z D 2002 *Phys. Rev.* B **65** 144527
[47] Trunin M R 2005 *Phys.—Usp.* **48** 979